European Congress on Computational Methods in Applied Sciences and Engineering
ECCOMAS 2000
Barcelona, 11-14 September 2000

INTERFACE CRACK PROPAGATION BETWEEN A POROUS-DUCTILE MATERIAL AND A RIGID SUBSTRATE

M. Cristina Porcu, Enrico Radi

Dipartimento di Ingegneria Strutturale
Università di Cagliari, Piazza D'Armi, 09123 Cagliari, Italy.
e-mail: mcporcu@hotmail.com, radi@vaxca1.unica.it

Key words: Fracture mechanics, interface crack propagation, elastic-plastic material, porous material, asymptotic analysis.

Abstract. *Along the interfaces between ductile and brittle materials a slow, stable crack growth is often observed before the crack propagates into one of the two materials. In the present work, a numerical asymptotic solution is provided for the stress and velocity fields near the tip of an interface crack, steadily propagating between a porous elastic-plastic material and a rigid substrate, under plane strain conditions. The Gurson model with constant and uniform porosity distribution and isotropic hardening is assumed for the constitutive description of the ductile material. This model may accurately describe the behavior of incompletely sintered porous metals and particulate-reinforced metal matrix composites. In analogy with the problem of interface crack growth in fully dense elastic-plastic materials, two distinct kinds of solution can be found in variable-separable form, corresponding to predominantly tensile or shear mixed mode. These solutions exist only if the hardening coefficient is lower than a critical value. For higher values the solution may display a complex stress singularity, as for the problem of an interface crack between linear elastic materials. In any case, if the ductile material is elastically incompressible then the Dugdale parameter vanishes and variable-separable crack-tip fields can be found for every set of the material parameters.*

Due to the higher hydrostatic stress state, the porosity influences only the stress fields of the tensile mode significantly. In particular, for high porosities the maximum of the hoop stress deviates from the interface line ahead of the crack-tip towards the porous ductile material, causing possible kinking of the fracture, so that the toughness of the interface crack may increase significantly. Therefore, the performed analysis of debonding process of this kind of interface results to be essential for the determination of the overall strength, toughness and reliability of many advanced composite materials.

1. INTRODUCTION

Interfaces between porous ductile metals and brittle layers are common in many advanced engineering materials obtained by compaction and sintering of metal and ceramic powders or formed by multi-layer substrates, like modern structural metallic/ceramic composites and packaging structures for electronic devices. This kind of interfaces specifically occurs in protective coatings of sintered metal components, where thin hard wear-resistant layers of titanium nitride (TiN), titanium carbonitride (TiC), alumina (Al_2O_3) or zirconia (ZnO), are deposited on the surface of these components in order to protect them from wear, high temperatures, chemical attack and corrosion. The use of protective coatings has been largely increased over the last years, since it may enhance the performance and extend the service life of many advanced structural components. In particular, an intensive employ has been made in a wide area of industrial applications, which range from gas turbine technology to aircraft and electronics industries, including several engineering applications, like filters, bearings, pumps, compressors, gears and cutting and forming tools. As well known, the properties of these components on a macroscopic scale depend on the adhesion and microstructure of the interfaces, since a commonly encountered kind of damage in the failure of layered composites is represented by slow, stable crack propagation along the interface. Therefore, in order to fully exploit the advantages of layered structural composites and protective coatings in improving the strength, toughening and surface properties of many engineering components, it becomes necessary to understand more thoroughly the detailed mechanisms by which fracture may growth and propagate along the interface between a porous ductile metal and a stiffer material.

The near-tip asymptotic fields for a crack steadily growing along a ductile/brittle interface have been investigated by several authors. In particular, the problem of interface crack propagation between an elastic-perfectly plastic material, obeying the von Mises yield condition, and a brittle substrate, assumed to be rigid for the sake of simplicity, has been studied by using limit analysis theory[1,2]. Moreover, the analysis has been extended to the interface between a ductile material characterized by the J_2-flow theory of plasticity, with linear strain hardening, and an isotropic linear elastic material[3]. These analyses show that two families only of solutions are possible near the growing crack-tip, under plane strain conditions. The first one displays a stress field mainly of the tensile type (Mode I-like), while the other one is prevalently of the shear type (Mode II-like). Moreover, if the Dugdale parameter is different from zero, a solution in variable-separable form exists only if the hardening coefficient is lower than a critical value[3]. Recently, the problem has been generalized by considering the plane stress condition[4] and the dynamic effects[5].

The problem of a stationary crack in a homogeneous porous ductile metal has been initially addressed[6-7] and recently extended to steadily crack propagation[8], also for linear hardening behavior[9,10]. All these analyses consider a constant porosity version of the Gurson constitutive model[11-13], which may accurately describe the behavior of incompletely sintered porous metals and particulate-reinforced metal matrix composites. The assumption of constant porosity may be reasonable out of the very near crack-tip zone, where micro-inhomogeneities, cavitation and finite deformation effects dominate. When a nucleation law for the porosity is

included, the crack-tip fields may not admit a variable-separable form and their determination may require finite element investigations. In any case, the evaluation of the asymptotic crack-tip fields gives important information about the debonding process and can also be used in conjunction with finite element simulations[14,15].

The objective of the present work is to study the steady-state crack propagation along the interface between a porous ductile material, perfectly bounded to a brittle substrate, which is modeled as rigid. In particular, an asymptotic analysis of the crack-tip fields is carried out in order to obtain detailed information on the structure of the local stress and deformation fields, and, thus, on the toughening mechanisms associated with the interface. The performed analysis follows the approach previously employed for the analysis of crack growth in homogeneous porous ductile media[9,10]. The results elucidate the effects of the constitutive parameters on the crack-tip fields, as well as the role played by the porosity in the stability of the crack propagation and in the occurrence of straight-ahead propagation or kinking. In analogy with the results for fully dense material[3], two distinct kinds of solution are found, corresponding to mainly tensile or shear crack-tip stress fields. However, due to the higher hydrostatic stress component, the effect of porosity is more pronounced for the tensile solution, rather than for the shear solutions. Previous findings can be obtained as special cases of the present formulation. In particular, for vanishing small porosities the ductile material coincides with the fully dense matrix material and the results recover those obtained for the J_2-flow theory displaying linear isotropic hardening[3]. Moreover, when the hardening modulus tends to vanish the results obtained from the limit analysis theory[1,2] are approached.

2. CONSTITUTIVE EQUATIONS

Reference is made to the Gurson model[11,12] of elastic-plastic solids containing spherical voids. The model is based on a yield surface having the form $\varphi(\sigma, \sigma_m, \phi) = 0$, where ϕ is the volume fraction of voids, σ is the average macroscopic stress tensor and the internal variable σ_m denotes the current flow stress of the matrix. By considering a constant porosity, the yield condition is taken in the form:

$$f(\sigma, \sigma_m) = \frac{3\,|dev\,\sigma|^2}{2\,\sigma_m^2} + 2\,\phi\,cosh\left(\frac{tr\,\sigma}{2\,\sigma_m}\right) - (1+\phi^2) = 0, \qquad (1)$$

where $dev\,\sigma$ and $tr\,\sigma$ denote the deviatoric part and the trace of σ, respectively. A generalization of the yield function in (1) could be easily included[13,16], but, for the sake of simplicity, is not considered here. Moreover, the growth and nucleation of voids has been neglected and the void volume fraction ϕ is assumed constant[6-10], so that the condition of associated plastic flow law for the matrix material implies an associated plastic flow law for the macroscopic porous material. Therefore, by assuming an elastic-plastic behavior displaying linear and isotropic hardening, the incremental constitutive equations relating the stress rate $\dot{\sigma}$ to the velocity of deformation $\dot{\varepsilon}$, result in [9,10]:

$$\dot{\varepsilon} = \frac{1}{E}\left[(1+\nu)\,\dot{\sigma} - \nu\,(tr\dot{\sigma})\,\mathbf{I} + \frac{\langle \mathbf{Q}\bullet\dot{\sigma}\rangle}{H}\,\mathbf{Q}\right], \tag{2}$$

where E and ν are the elastic Young modulus and Poisson ratio of the matrix material, respectively. The MacAuley brackets are defined such that $\langle x\rangle = Sup\{x, 0\}$ for every real value x, and **Q** is a second order tensor proportional to the gradient of the yield function (1), namely:

$$\mathbf{Q} = \frac{\sigma_m}{2}\,\frac{\partial f}{\partial \sigma} = \frac{3}{2\,\sigma_m}\,dev\,\sigma + \frac{\phi}{2}\,sinh\left(\frac{tr\,\sigma}{2\,\sigma_m}\right)\mathbf{I}. \tag{3}$$

The hardening modulus H of the macroscopic porous material turns out to be[9]:

$$H = \frac{\alpha E}{(1-\alpha)}\,\frac{(\mathbf{Q}\cdot\sigma)^2}{(1-\phi)\,\sigma_m^2}, \tag{4}$$

where $\alpha = E_t / E$, and E_t is the current longitudinal modulus of the matrix material. From (4), it can be noted that a positive hardening ($0 < \alpha < 1$) of the matrix material results in a positive hardening modulus H of the porous material, since the dot product $\mathbf{Q}\bullet\sigma$ vanishes if and only if $\sigma = \mathbf{0}$, which may occur inside the yield locus only.

Moreover, the rate of growth of the yield surface, measured by $\dot{\sigma}_m$, results in[9,10]:

$$\dot{\sigma}_m = \frac{\langle \mathbf{Q}\cdot\dot{\sigma}\rangle}{\mathbf{Q}\cdot\sigma}\,\sigma_m. \tag{5}$$

In the following, it will be assumed that the incremental constitutive equations (2) and (5) hold when the stress state satisfies the yield condition (1), whereas an elastic isotropic constitutive behavior is considered during elastic unloading.

3. INTERFACE CRACK PROPAGATION

The problem of a plane crack propagating at constant velocity *c* along a rectilinear interface between a porous ductile medium and a rigid substrate is considered (Fig. 1). A cylindrical coordinate system (r, ϑ, x_3) moving with the crack-tip towards the $\vartheta = 0$ direction is considered, with the x_3-axis along the straight crack front.

The mechanical behavior of the elastic-plastic material is described by the rate constitutive laws (2) and (5). This framework allows considering elastic unloading sectors, which may appear in the proximity of the crack-tip during crack propagation.

The steady-state condition yields the following time derivative rule, for any scalar function $\phi(r, \vartheta)$:

$$\dot{\phi} = \frac{c}{r}\,(\phi_{,\vartheta}\sin\vartheta - r\,\phi_{,r}\cos\vartheta). \tag{6}$$

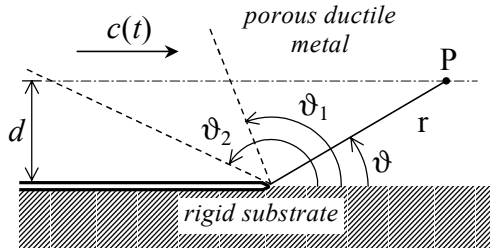

Figure 1. Cylindrical co-ordinate system centered at the moving interface crack-tip and trajectory of the material point P through elastic and plastic sectors, bounded by angles ϑ_1 and ϑ_2.

The conditions of kinematics compatibility for infinitesimal deformations and quasi-static equilibrium imply:

$$\dot{\varepsilon} = \tfrac{1}{2}(\nabla \mathbf{v} + \nabla \mathbf{v}^{\mathsf{T}}), \tag{7}$$

$$div\, \sigma = 0.$$

Moreover, the plane strain condition $\dot{\varepsilon}_{33} = 0$ must be also considered.

Compatibility (7_1), equilibrium (7_2) and constitutive incremental equations (2.2) and (2.5) form a first order PDEs system, which governs the problem of the crack propagation. The solution can be searched in variable-separable form, by considering single term asymptotic expansions of near crack-tip fields. In particular, the stress, velocity, and flow stress fields are assumed in the form:

$$\mathbf{v}(\mathrm{r}, \vartheta) = -\frac{c}{s}\left(\frac{\mathrm{r}}{\mathrm{B}}\right)^{s} \mathbf{w}(\vartheta), \tag{8}$$

$$\sigma(\mathrm{r}, \vartheta) = \mathrm{E}\left(\frac{\mathrm{r}}{\mathrm{B}}\right)^{s} \mathbf{T}(\vartheta),$$

$$\sigma_m(\mathrm{r}, \vartheta) = \mathrm{E}\left(\frac{\mathrm{r}}{\mathrm{B}}\right)^{s} \mathrm{T}_m(\vartheta),$$

where s denotes the (negative) exponent of the stress singularity, and B is a characteristic dimension of the plastic zone, which remains undetermined by the asymptotic analysis, since the lower order problem is homogeneous. Nevertheless, the amplitude of the asymptotic fields can be estimated by a matching procedure with the findings of a full-field analysis performed, e.g., by the finite element method[14,15].

The introduction of the asymptotic stress fields (8_2) into equilibrium equations (7_2), yields the following two ODEs:

$$\mathrm{T}_{\mathrm{r}\vartheta,\vartheta} = -(1+s)\,\mathrm{T}_{\mathrm{rr}} + \mathrm{T}_{\vartheta\vartheta}, \tag{9}$$

$$\mathrm{T}_{\vartheta\vartheta,\vartheta} = -(2+s)\,\mathrm{T}_{\mathrm{r}\vartheta}.$$

The rates of the fields ε, σ and σ_m may be consequently assumed in the form:

$$\dot{\varepsilon} = -\frac{c}{s\,\mathrm{r}}\left(\frac{\mathrm{r}}{\mathrm{B}}\right)^{s}\mathbf{D}(\vartheta), \tag{10}$$

$$\dot{\sigma} = \frac{c\,\mathrm{E}}{\mathrm{r}}\left(\frac{\mathrm{r}}{\mathrm{B}}\right)^{s}\Sigma(\vartheta),$$

$$\dot{\sigma}_{m} = \frac{c\,\mathrm{E}}{\mathrm{r}}\left(\frac{\mathrm{r}}{\mathrm{B}}\right)^{s}\Sigma_{m}(\vartheta),$$

where the components of $\mathbf{D}$, Σ, and Σ_m are functions of the angular coordinate ϑ. In particular, by using the derivative rule (6) and equilibrium relations (9), the cylindrical components of Σ and Σ_m assume the following expressions:

$$\begin{aligned}
\Sigma_{r\vartheta} &= -\,s\,(\mathrm{T}_{rr}\,sin\,\vartheta + \mathrm{T}_{r\vartheta}\,cos\,\vartheta), \\
\Sigma_{\vartheta\vartheta} &= -\,s\,(\mathrm{T}_{r\vartheta}\,sin\,\vartheta + \mathrm{T}_{\vartheta\vartheta}\,cos\,\vartheta), \\
\Sigma_{rr} &= (\mathrm{T}_{rr,\vartheta} - 2\,\mathrm{T}_{r\vartheta})\,sin\,\vartheta - s\,\mathrm{T}_{rr}\,cos\,\vartheta, \\
\Sigma_{33} &= \mathrm{T}_{33,\vartheta}\,sin\,\vartheta - s\,\mathrm{T}_{33}\,cos\,\vartheta, \\
\Sigma_{m} &= \mathrm{T}_{m,\vartheta}\,sin\,\vartheta - s\,\mathrm{T}_{m}\,cos\,\vartheta.
\end{aligned} \tag{11}$$

Moreover, the compatibility relation (7_1) yields:

$$\begin{aligned}
\mathrm{D}_{rr} &= s\,\mathrm{w}_{r}, \\
\mathrm{D}_{\vartheta\vartheta} &= \mathrm{w}_{\vartheta,\vartheta} + \mathrm{w}_{r}, \\
\mathrm{D}_{r\vartheta} &= \frac{1}{2}\,[\mathrm{w}_{r,\vartheta} - (1-s)\,\mathrm{w}_{\vartheta}].
\end{aligned} \tag{12}$$

It is worth noting that, when the asymptotic stress fields ($8_{2,3}$) are introduced in (1) and (3), the yield function f and its gradient $\mathbf{Q}$ turn out to be independent of r, so that they may be written in the equivalent form:

$$f(\mathbf{T}, \mathrm{T}_{m}) = \frac{3\,|\,dev\,\mathbf{T}\,|^{2}}{2\,\mathrm{T}_{m}^{2}} + 2\,\phi\,cosh\left(\frac{tr\,\mathbf{T}}{2\,\mathrm{T}_{m}}\right) - (1+\phi^{2}) = 0, \tag{13}$$

$$\mathbf{Q} = \frac{3}{2\,\mathrm{T}_{m}}\,dev\,\mathbf{T} + \frac{\phi}{2}\,sinh\left(\frac{tr\,\mathbf{T}}{2\,\mathrm{T}_{m}}\right)\mathbf{I}.$$

As a consequence of (8) and (10), the dimensionless hardening modulus of the porous material h = H/E becomes:

$$h = \frac{\alpha}{(1-\alpha)}\,\frac{(\mathbf{Q}\bullet\mathbf{T})^{2}}{(1-\phi)\,\mathrm{T}_{m}^{2}}. \tag{14}$$

A substitution of the asymptotic fields (8) and their rates (10) into the incremental constitutive relationships (2) and (5) by using (12) yields the following system of five equations:

$$w_{r,\vartheta} = (1-s)\, w_\vartheta - 2s\,[(1+\nu)\,\Sigma_{r\vartheta} + \lambda\, Q_{r\vartheta}], \tag{15}$$

$$w_{\vartheta,\vartheta} = -w_r - s\,[\Sigma_{\vartheta\vartheta} - \nu\,(\Sigma_{rr} + \Sigma_{33}) + \lambda\, Q_{\vartheta\vartheta}],$$

$$\Sigma_{rr} - \nu\,(\Sigma_{\vartheta\vartheta} + \Sigma_{33}) + \lambda\, Q_{rr} + w_r = 0,$$

$$\Sigma_{33} - \nu\,(\Sigma_{\vartheta\vartheta} + \Sigma_{rr}) + \lambda\, Q_{33} = 0,$$

$$T_{m,\vartheta}\, sin\,\vartheta = (s\, cos\,\vartheta + \frac{\lambda\, h}{\mathbf{Q}\cdot\mathbf{T}})\, T_m, \tag{16}$$

where

$$\lambda = \langle \mathbf{Q} \bullet \Sigma \rangle / h, \tag{17}$$

if the stress fields meet the yield condition (13), else $\lambda = 0$. During elastic unloading or neutral loading, the constitutive relations (15) reduce to the incremental equations of linear isotropic elasticity, recovered for $\lambda = 0$, and equation (16) becomes equivalent to the condition $\dot{\sigma}_m = 0$. Equations (15) and (16), together with the equilibrium equations (9), result in seven homogeneous first order ODEs, for the seven unknown angular functions w_r, w_ϑ, $T_{r\vartheta}$, T_{rr}, $T_{\vartheta\vartheta}$, T_{33} and T_m. It is worth noting that the unknown exponent s may be determined as an eigenvalue of the non-linear problem[17], by considering a normalization condition for the solution.

In order to employ a numerical integration procedure, the ODEs (15) should be transformed in explicit form. In particular, from ($15_{3,4}$) the following system of equations may be derived:

$$(h + Q_{rr}^2)\,\Sigma_{rr} - (\nu h - Q_{rr}\, Q_{33})\,\Sigma_{33} = -w_r\, h + (\nu h - Q_{rr}\, Q_{\vartheta\vartheta})\,\Sigma_{\vartheta\vartheta} - 2\, Q_{rr}\, Q_{r\vartheta}\,\Sigma_{r\vartheta}, \tag{18}$$

$$(\nu h - Q_{rr}\, Q_{33})\,\Sigma_{rr} - (h + Q_{33}^2)\,\Sigma_{33} = 2\, Q_{33}\, Q_{r\vartheta}\,\Sigma_{r\vartheta} - (\nu h - Q_{33}\, Q_{\vartheta\vartheta})\,\Sigma_{\vartheta\vartheta}.$$

Equations ($11_{1,2}$) make clear that $\Sigma_{r\vartheta}$ and $\Sigma_{\vartheta\vartheta}$ do not depend on the derivatives of the unknown functions, and so the right hand sides of (18). Therefore, equations (18) may be solved for Σ_{rr} and Σ_{33}. In particular, Σ_{rr} turns out to be:

$$\Sigma_{rr} = \frac{1}{\Delta}\left\{\Sigma_{\vartheta\vartheta}\,[\nu(1+\nu)h + \nu Q_{33}\,(Q_{33} - Q_{\vartheta\vartheta}) - Q_{rr}\,(\nu Q_{33} + Q_{\vartheta\vartheta})] - 2\,\Sigma_{r\vartheta}\, Q_{r\vartheta}\,(\nu Q_{33} + Q_{rr}) - w_r\,(h + Q_{33}^2)\right\}, \tag{19}$$

where:

$$\Delta = (1-\nu^2)\, h + Q_{33}^2 + Q_{rr}^2 + 2\,\nu\, Q_{rr}\, Q_{33}, \tag{20}$$

is always greater than zero. Being Σ_{rr} known from (19), Σ_{33} may be obtained from a rearrangement of (18_2). When Σ_{rr} and Σ_{33} are substituted into ($11_{3,4}$), the derivatives of the stress components T_{rr} and T_{33} with respect to the angular co-ordinate ϑ may be obtained:

$$T_{rr,\vartheta} = 2\,T_{r\vartheta} + (s\,T_{rr}\,cos\,\vartheta + \Sigma_{rr}) / sin\,\vartheta, \tag{21}$$

$$T_{33,\vartheta} = (s\,T_{33}\,cos\vartheta + \Sigma_{33}) / sin\,\vartheta.$$

Then, the expressions for $w_{r,\vartheta}$ and $w_{\vartheta,\vartheta}$ follow from the constitutive relations $(15_{1,2})$.

Equations (9), $(15_{1,2})$-(16) and (21) form the first order ODEs system, which governs the near-tip stress and velocity fields. This system may be written in the explicit form:

$$\mathbf{y}'(\vartheta) = \begin{cases} \mathbf{f}_p(\vartheta, \mathbf{y}(\vartheta), s) & if \quad f(\mathbf{T}, T_m) = 0 \quad and \quad \mathbf{Q} \cdot \Sigma > 0, \\ \mathbf{f}_e(\vartheta, \mathbf{y}(\vartheta), s) & if \quad f(\mathbf{T}, T_m) < 0 \quad or \quad f(\mathbf{T}, T_m) = 0 \; and \; \mathbf{Q} \cdot \Sigma \le 0, \end{cases} \tag{22}$$

where the vector:

$$\mathbf{y} = \{w_r,\, w_\vartheta,\, T_{r\vartheta},\, T_{rr},\, T_{\vartheta\vartheta},\, T_{33},\, T_m\}. \tag{23}$$

collects the unknown velocity and stress functions of the angular co-ordinate ϑ.

3.1. Elastic unloading and secondary plastic reloading

Under the assumption of small deformations, the motion of a generic material point P close to the trajectory of the crack-tip is assumed to occur along a straight path at a fixed distance, say *d*, from the interface crack line (Fig. 1). The angular co-ordinate ϑ singles out the position of the material point moving along its rectilinear path, defined by the geometric relation:

$$r(\vartheta) = d / sin\,\vartheta. \tag{24}$$

As the crack-tip approaches and, then, goes beyond the material point, the point experiences plastic loading, elastic unloading and subsequent plastic reloading. In particular, the material point, initially ahead of the crack-tip, leaves the plastic loading sector at the elastic unloading angle ϑ_1 where the plastic multiplier λ vanishes, namely when:

$$\mathbf{Q}(\vartheta_1) \bullet \Sigma(\vartheta_1) = 0. \tag{25}$$

Throughout the elastic unloading sector the plastic multiplier λ vanishes, the rate constitutive law (15) reduces to the usual linear isotropic elastic relation and the current flow stress σ_m of the point remains constant and equal to the value assumed at the elastic unloading angle ϑ_1. Plastic reloading on crack flanks occurs at the angle ϑ_2 where the point reaches a stress state lying on the yield surface left at unloading, that is:

$$f\,\{\sigma[r(\vartheta_2), \vartheta_2], \sigma_m\,[r(\vartheta_1), \vartheta_1]\} = 0. \tag{26}$$

4. INTERFACE BOUNDARY CONDITIONS

The rigid interface implies the vanishing of the velocity functions along the interface plane at ϑ=0, namely:

$$w_\vartheta(0) = w_r(0) = 0, \tag{27}$$

whereas the free crack surface at $\vartheta=\pi$ implies the following conditions on the stress functions:

$$T_{\vartheta\vartheta}(\pi) = T_{r\vartheta}(\pi) = 0. \tag{28}$$

By using the boundary conditions (27) and relations (11) evaluated at $\vartheta=0$, the constitutive equations (15) become:

$$\begin{aligned} w_{r,\vartheta}(0) &= 2\, s^2\, (1+\nu)\, T_{r\vartheta}(0) - 2\, s\, \lambda(0)\, Q_{r\vartheta}(0), \\ w_{\vartheta,\vartheta}(0) &= s^2\, \{T_{\vartheta\vartheta}(0) - \nu[T_{rr}(0) + T_{33}(0)]\} - s\, \lambda(0)\, Q_{\vartheta\vartheta}(0), \\ -s\, &\{T_{rr}(0) - \nu\, [T_{33}(0) + T_{\vartheta\vartheta}(0)]\} + \lambda(0)\, Q_{rr}(0) = 0, \\ -s\, &\{T_{33}(0) - \nu\, [T_{rr}(0) + T_{\vartheta\vartheta}(0)]\} + \lambda(0)\, Q_{33}(0) = 0, \end{aligned} \tag{29}$$

where $\mathbf{Q}(0)$ and $\lambda(0)$ may be evaluated from (13_2) and (17):

$$\mathbf{Q}(0) = \frac{3}{2\, T_m(0)}\, dev\, \mathbf{T}(0) + \frac{\phi}{2}\, sinh\left(\frac{tr\mathbf{T}(0)}{2\, T_m(0)}\right)\mathbf{I}, \tag{30}$$

$$\lambda(0) = -s\, \frac{(1-\alpha)}{\alpha}\, \frac{(1-\phi)\, T_m^2(0)}{\mathbf{Q}(0)\bullet\mathbf{T}(0)}. \tag{31}$$

Note that the product:

$$\mathbf{Q}(0)\bullet\mathbf{T}(0) = \frac{3}{2\, T_m(0)}\, |\, dev\, \mathbf{T}(0)\,|^2 + \frac{\phi}{2}\, [tr\, \mathbf{T}(0)]\, sinh\left(\frac{tr\mathbf{T}(0)}{2\, T_m(0)}\right), \tag{32}$$

is always positive, since $\mathbf{T}(0) \neq \mathbf{0}$. It follows that $\lambda(0) > 0$, i.e. along the interface ahead of the crack-tip the ductile material undergoes plastic loading.

By taking the difference between equations (29_3) and (29_4) it may be found that:

$$\left[\frac{3\, \lambda(0)}{2\, T_m(0)} - s\, (1-\nu)\right]\, [T_{rr}(0) - T_{33}(0)] = 0. \tag{33}$$

Since the first term in (33) is always positive, it follows that $T_{33}(0) = T_{rr}(0)$ and thus:

$$\begin{aligned} tr\, \mathbf{T}(0) &= T_{\vartheta\vartheta}(0) + 2\, T_{rr}(0), \\ |\, dev\, \mathbf{T}(0)|^2 &= \frac{2}{3}\, \{[T_{\vartheta\vartheta}(0) - T_{rr}(0)]^2 + 3\, T_{r\vartheta}(0)^2\}. \end{aligned} \tag{34}$$

In order to solve the system of ODEs (22) the Runge-Kutta procedure is used (IMSL subroutine DIVPRK). This approach requires the knowledge of $\mathbf{y}(0)$. However, the boundary conditions do not specify the stress components at $\vartheta = 0$, and thus, their values must be preliminarily defined. Firstly, the normalization condition $T_m(0) = 1$ is adopted to avoid the trivial solution due to the homogeneous boundary conditions (27) and (28). Then, $T_{r\vartheta}(0)$ is obtained from the yield condition (13_1) evaluated at $\vartheta = 0$:

$$T_{r\vartheta}(0)^2 = \frac{1}{3}\{1 + \phi^2 - 2\,\phi\, cosh\,[0.5\,T_{\vartheta\vartheta}(0) + T_{rr}(0)] - [T_{\vartheta\vartheta}(0) - T_{rr}(0)]^2\}, \qquad (35)$$

which admits two distinct and opposite roots. Moreover, the position:

$$p = T_{rr}(0)/T_{\vartheta\vartheta}(0), \qquad (36)$$

is made and the value of $T_{\vartheta\vartheta}(0)$ is found as an implicit function of p by solving the non-linear algebraic equation obtained from the constitutive relation (29_3), by using (35) and (36):

$$1 + \phi^2 - 2\,\phi\, cosh\,\xi + \phi\,\xi\, sinh\,\xi + \frac{(1-\phi)(1-\alpha)}{2\alpha[(1-\nu)p-\nu]}[(p+0.5)\,\phi\,\frac{sin\,\xi}{\xi} + p - 1] = 0, \qquad (37)$$

where:

$$\xi = (p + 0.5)\,T_{\vartheta\vartheta}(0). \qquad (38)$$

Note that equation (37) admits at least two opposite roots for ξ, which are numerically detected (IMSL subroutine DZBREN).

The unknown values of s and p are numerically calculated by the following iterative procedure, based on the achievement of the boundary conditions (28). The integration of the ODEs system (22) is initially performed by assuming arbitrary values for p and s. Then, the corresponding values of $T_{rr}(0)$, $T_{\vartheta\vartheta}(0)$ and $T_{r\vartheta}(0)$ are found from equations (35)-(37) and, thus, the components of $\mathbf{y}(0)$ are fully defined, so that the numerical integration procedure may start. On the basis of a check on the values of $T_{\vartheta\vartheta}(\pi)$ and $T_{r\vartheta}(\pi)$, the guessed values of p and s are reassigned and the process is iterated using a modified Powell hybrid method (IMSL subroutine DNEQNF), until $T_{\vartheta\vartheta}(\pi)$ and $T_{r\vartheta}(\pi)$ turn out to be sufficiently close to zero as required by (28). Finally, all the fields are normalised through the condition $T_m(\vartheta_1) = 1$.

The choice of the right sign for the values of $T_{r\vartheta}(0)$ and ξ resulting from (35) and (37) depends on the sign obtained at the end of the integration procedure for the velocity component $w_\vartheta(\pi)$, which must be negative or null to avoid interface crack closure.

5. RESULTS AND CONCLUSIONS

Two distinct solutions have been found with slightly different values of the stress singularity and very different, but fixed, mixities of the local crack-tip fields, corresponding to predominantly tensile or shear stress field. Therefore, the discrete near-tip mode mix turns out to be independent of the remote mode mix. This is consistent with the results obtained for full densities of the ductile material[1-5], which may be recovered by the present analysis for $\phi = 0$. It is worth noting that two further solutions have been detected with the same singularities but opposite values of the crack-tip fields. However, these solutions have been rejected since their velocity fields correspond to interface crack closure.

In analogy with the problem of interface crack growth in fully dense elastic-plastic materials[3], the solution can be found in variable-separable form only if the hardening coefficient α is lower than a critical value, which depends on the Poisson coefficient ν

through the Dugdale parameter ε evaluated for the case of a rigid interface:

$$\varepsilon = \frac{1}{2\pi}\, ln\,(3 - 4\,\nu). \tag{39}$$

This occurrence is consistent with the problem of an interface crack between linear elastic materials[18], for which the stress singularity is complex of the form $s = -0.5 + i\,\varepsilon$. In particular, if the material is elastically incompressible, namely for ν=0.5, the parameter ε in (39) vanishes and the solution can be found for every value of α ranging between 0 and 1. The results reported in the following have been obtained for the value ν=0.3, which corresponds to a critical value of α close to 0.275. Note that the present analysis does not exclude the existence of solutions different from those in variable-separable form, which could be detected by a full field numerical analysis. However, the finite element investigations[14] performed for vanishing porosity (ϕ=0) confirmed the predictions of the asymptotic analysis[3] and so is expected for porous ductile metals.

The effects of porosity on the stress singularity *s*, elastic unloading ϑ_1 and plastic reloading ϑ_2 angles are outlined in Figs. 2-4 for both tensile and shear solutions and for two distinct values of the linear hardening parameter, namely α=0.01 and α=0.1. The results presented in Fig. 2 for the tensile solution show that the strength of the stress singularity, given by the absolute value of *s*, increases with respect to the case of fully dense material (ϕ=0). The increase of singularity generally turns out to be an instabilizing effect on the interface crack propagation. However, the singularity attains a maximum at intermediate values of porosity and then decreases, so that a greater propensity for stable crack growth occurs for higher porosities. A different trend may be observed for the shear mode. In this case the singularity decreases almost linearly, so that the crack propagation becomes more and more stable as the porosity increases. Note that for low porosities the tensile solution has a lower singularity with respect to the shear mode. In this case, the shear state may be unstable and may be regarded as a transitory state towards a more stable state of near-tip tension, as already observed in the small scale yielding analysis[14] performed for ϕ = 0. On the contrary, for high porosities the shear solution has a lower singularity, so that it may result more stable than the tensile mode.

From Fig. 3 it may be noted that for tensile mode the size of the elastic unloading sector (E) in proximity of the crack-tip enlarges as the porosity increases, so that the plastic deformation tends to concentrate ahead of the crack-tip. Unlike tensile mode, for shear mode the porosity has low effects on the extension of elastic (E) and plastic (P) sectors, see Fig.4, except for the size of a secondary plastic loading sector, which arises within the elastic unloading sector for high hardening values.

The angular variations of the asymptotic fields for the components of the stress tensor **T** and for the current flow stress T_m are plotted in Fig. 5, for both tensile (a, b) and shear (c, d) modes. These plots refer to the low hardening coefficient α=0.01 and to the values of porosity ϕ=0.001 and ϕ=0.1.

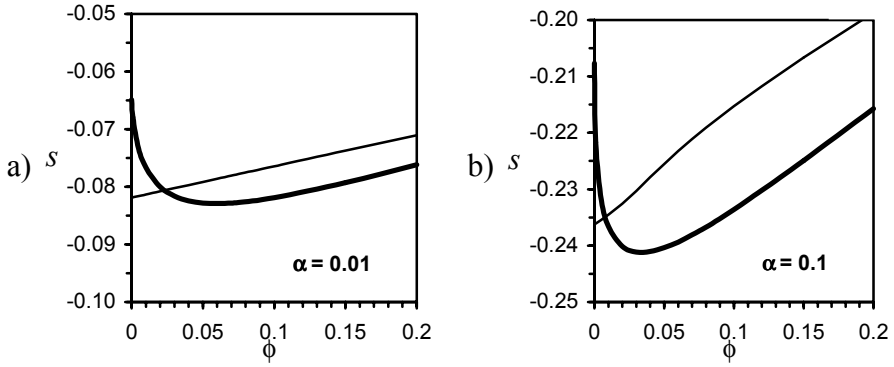

Figure 2. Strength of the stress singularity *s* under tensile (bold curve) and shear (solid curve) modes, for ν=0.3 and two distinct values of α.

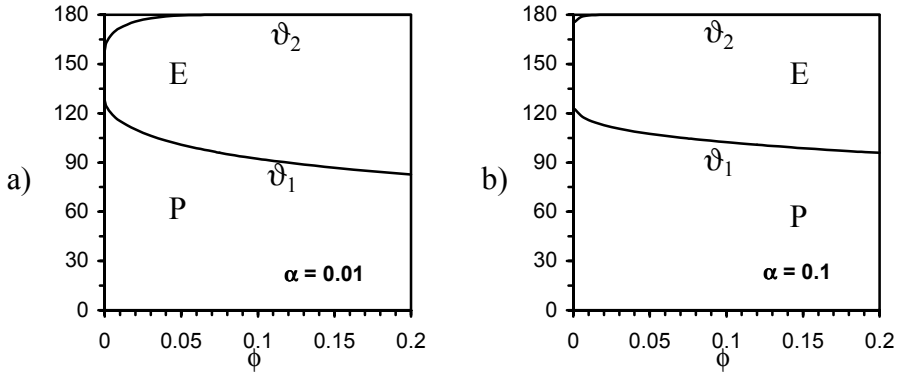

Figure 3. Elastic unloading ϑ_1 and plastic reloading ϑ_2 angles as functions of porosity for tensile solution, ν=0.3 and two distinct values of α.

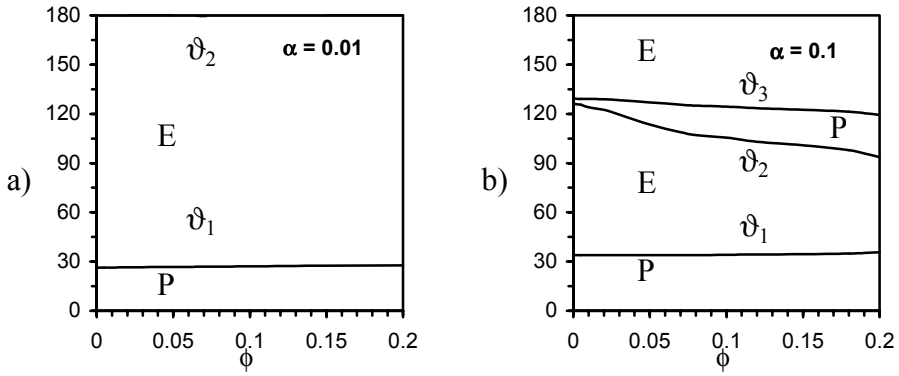

Figure 4. Elastic unloading ϑ_1 and ϑ_3 and plastic reloading ϑ_2 angles as functions of porosity for shear solution, ν=0.3 and two distinct values of α.

The results obtained in Fig. 5a for low porosity (ϕ=0.001) show that the tensile stress field ahead of the crack-tip is characterized by large stress triaxiality in the ductile material. In particular, the hydrostatic stress component ahead of the crack-tip exceeds more than three times the current flow stress. The stress fields in Fig. 5b, obtained for ϕ=0.1, show that the main effects of the porosity increase is a lowering of the mean stress, together with a decrease of the shear stress component $T_{r\vartheta}$, which becomes negative along the interface line at ϑ=0. Correspondingly, the location of the maximum hoop stress $T_{\vartheta\vartheta}$ for the tensile solution deviates from the interface line ahead of the crack-tip towards the porous ductile material. Precisely, the maximum is attained where the shear stress vanishes, as it follows from (9_2). This occurrence may cause possible kinking of the fracture trajectory, so that the interfacial toughness may significantly increase. The stress fields of the shear mode display positive, but very low, mean stress at ϑ=0, see Figs. 5c,d, thus resulting approximately in a Mode II solution. Therefore, the porosity influences mostly the stress fields of the tensile mode, as a consequence of the high hydrostatic stress level.

In the limit case of vanishing hardening the elastic-perfectly plastic behavior is approached, as can be noted from Fig 5 obtained for a low hardening coefficient (α=0.01). In this case, the near-tip stress fields tend to display for both modes a centered-fan sector starting from the rigid interface to the elastic unloading angle, followed by an elastic deformation sector and a constant stress plastic sector, as already found for fully dense ductile material obeying the von Mises yield condition[1-3]. Nevertheless, the problem of a crack growing between a porous elastic-perfectly plastic material and a rigid substrate has not yet been studied and will be the focus of a future investigation.

The angular variations of the Cartesian components of velocity are shown in Fig. 6 for the same hardening value (α=0.01). These plots show that the component of velocity w_2 evaluated at $\vartheta=\pi$ turns out to be positive for all the reported results, thus implying crack opening.

The angular variations of the tensile stress fields for the high hardening value of α=0.1 are reported in Figs. 7a,b. These results are roughly similar to those relevant to the low hardening case (α=0.01) plotted in Figs. 5a,b, except that the shear stress component at ϑ=0 is negative also for small porosity. On the contrary, the angular variation of the stress fields for shear mode, shown in Figs. 7c,d, turns out to be opposite in sign with respect to the low hardening case in Figs. 5c,d. In particular, along the interface line the shear stress component $T_{r\vartheta}$ is negative, while the hoop stress $T_{\vartheta\vartheta}$ remains tensile, leading thus to crack opening (see the angular variation of the velocity functions in Fig. 8). Note that solutions displaying near-tip fields opposite to those reported in Figs. 5-8 may also occur, but they imply crack closure and, therefore, have been rejected.

It is worth noting that linear isotropic hardening may represent an intermediate model between the limit cases of linear elastic and perfectly-plastic constitutive behavior and may adequately account for the dissipation of energy in the plastic zone near the crack-tip, which is responsible for stable crack growth. In any case, the rough model of isotropic hardening may be refined by the introduction of a more realistic mixed isotropic\kinematic hardening behavior, as already done for crack propagation in homogeneous porous ductile metals[10].

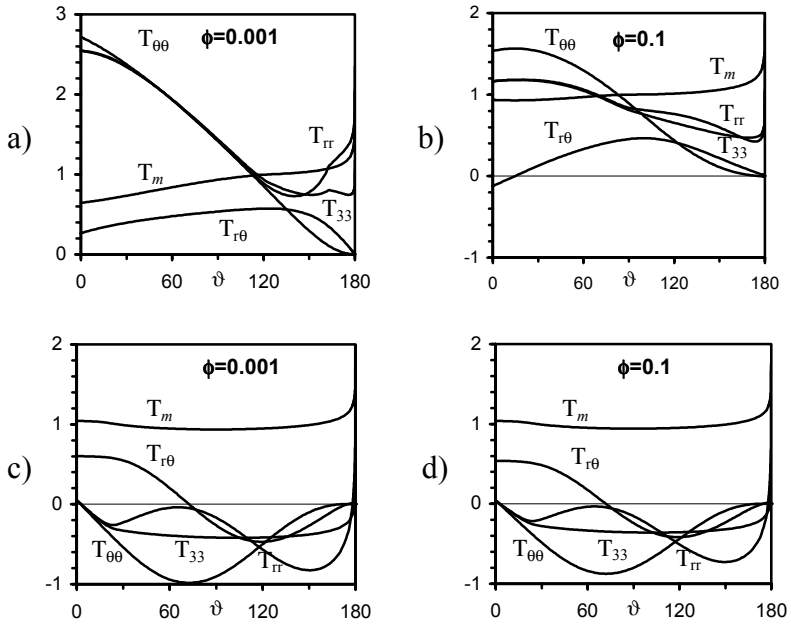

Figure 5. Angular variations of the stress fields near crack-tip under tensile (a, b) and shear (c, d) modes, for ν=0.3, α=0.01 and two distinct values of the porosity ϕ.

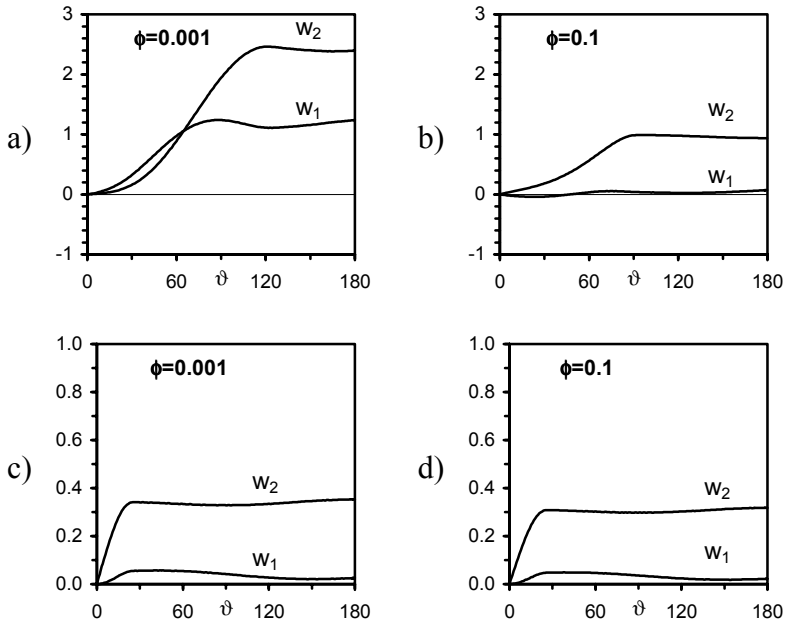

Figure 6. Angular variations of the velocity fields near crack-tip under tensile (a, b) and shear (c, d) modes, for ν=0.3, α=0.01 and two distinct values of the porosity ϕ.

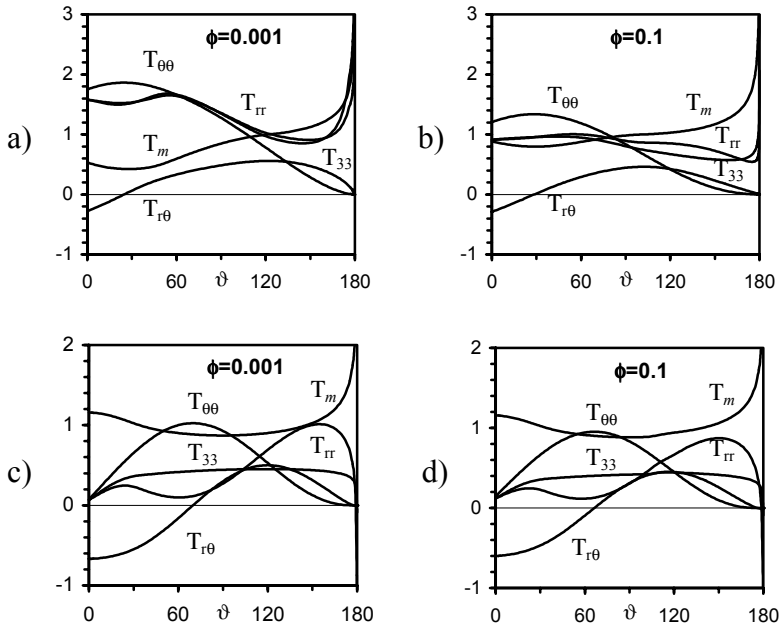

Figure 7. Angular variations of the stress fields near crack-tip under tensile (a, b) and shear (c, d) modes, for ν=0.3, α=0.1 and two distinct values of the porosity ϕ.

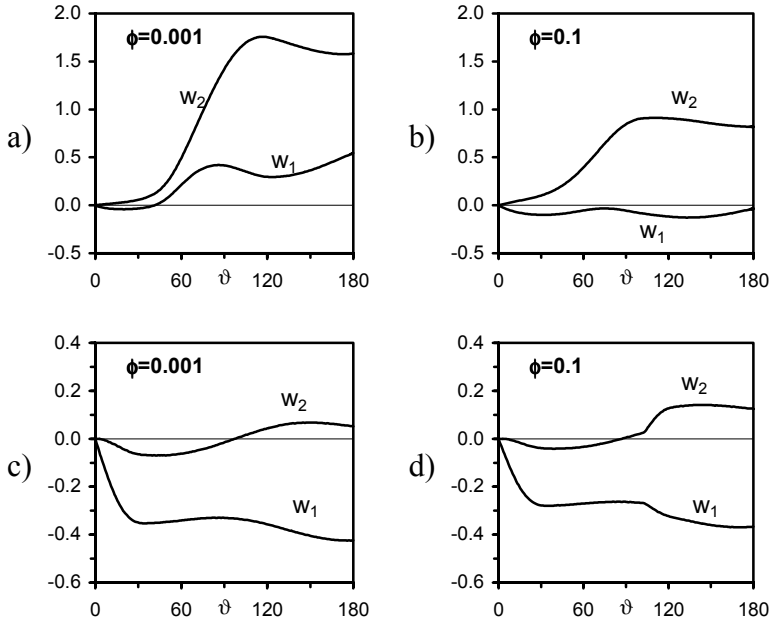

Figure 8. Angular variations of the velocity fields near crack-tip under tensile (a, b) and shear (c, d) modes, for ν=0.3, α=0.1 and two distinct values of the porosity ϕ.

In conclusion, the results of the present investigations show that an increase of porosity leads to significant modifications of the angular distribution of stress and velocity fields, together with a drastic reduction in the hydrostatic stress level, especially along the interfacial line. The performed near-tip asymptotic analysis predicts, rather accurately, the stress singularity and the near-tip mode mix for a crack between a porous ductile metal and a stiffer substrate. Moreover, it gives important information about the interfacial toughness and stability. Finally, the obtained results may be useful to check further numerical simulations performed, e.g., by the finite element method.

ACKNOWLEDGEMENTS

Financial support of M.U.R.S.T. ex60% (1999) "Propagazione di una frattura lungo l'interfaccia tra un materiale poroso ed un sottostrato rigido" is gratefully acknowledged.

REFERENCES

[1] Q. Guo and L. Keer, "A crack at the interface between an elastic-perfectly plastic solid and a rigid substrate", *J. Mech. Phys. Solids*, **38**, 843-857 (1990).

[2] W.J. Drugan, "Near-tip fields for quasi-static crack growth along a ductile-brittle interface", *J. Appl. Mech*., **58**, 111-119 (1991).

[3] P. Ponte Castañeda and P.A. Mataga, "Stable crack growth along a brittle/ductile interface – I. Near-tip fields", *Int. J. Solids Struct*., **27**, 105-133 (1991).

[4] H. Yuan, "Plane stress near-tip field analysis of steady-state crack growth along a linear-hardening elastic-plastic interface", *Acta Mech*., **109**, 207-226 (1995).

[5] H. Yuan, "Dynamic crack growth along an elastoplastic bimaterial interface", *Acta Mech*., **121**, 51-77 (1997).

[6] W.J. Drugan and Y. Miao, "Influence of porosity on plane strain tensile crack-tip stress fields in elastic-plastic materials: part I", *J. Appl. Mech.*, **59**, 559-567 (1992).

[7] Y. Miao and W.J. Drugan, "Influence of porosity on plane strain tensile crack-tip stress fields in elastic-plastic materials: part II", *J. Appl. Mech*., **60**, 883-889 (1993).

[8] Y. Miao and J.W. Drugan, "Asymptotic analysis of growing crack stress/deformation fields in porous ductile metals and implications for stable crack growth", *Int. J. Fracture*, **72**, 69-96 (1995).

[9] E. Radi and D. Bigoni, "On crack propagation in porous hardening metals", *Int. J. Plasticity*, **10**, 761-793 (1994).

[10] E. Radi and D. Bigoni, "Effects of anisotropic hardening on crack propagation in porous-ductile materials", *J. Mech. Phys. Solids*, **44**, 1475-1508 (1996).

[11] A.L. Gurson, *Porous rigid-plastic materials containing rigid inclusions- yield function, plastic potential and void nucleation*. Fracture, 2, ICF4, Waterloo, Canada (1977).

[12] A.L. Gurson, "Continuum theory of ductile rupture by void nucleation and growth: part I - yield criteria and flow rules for porous ductile media", *Int. J. Engng. Mat. Tech.*, **99,** 2-15 (1977).

[13] V. Tvergaard, "Material failure by void grouth to coalescence", *Adv. Appl. Mech*., **27**, 83-151 (1990).
[14] K. Bose, P.A. Mataga and P. Ponte Castañeda, "Stable crack growth along a brittle/ductile interface – II. Small scale yielding solution and interfacial toughness predictions", *Int. J. Solids Struct*., **36**, 1-34 (1999).
[15] S. Aoki, K. Kishimoto, N. Takeuchi and M. Sakata, "An elastic-plastic finite element analysis of a blunting interface crack with microvoid damage", *Int. J. Fracture*, **55**, 363-374 (1992).
[16] A. Needleman and V. Tvergaard, "An Analysis of Ductile Rupture Modes at a Crack", *J. Mech. Phys. Solids*, **35**, 151-183 (1987).
[17] K. Bose and P. Ponte Castañeda, "Stable crack growth under mixed mode conditions", *J. Mech. Phys. Solids*, **40**, 1053-1103 (1992).
[18] M.L. Williams, "The stress around a fault or a crack in dissimilar media", *Bull. Seism. Soc. Am.*, **49**, 199-204 (1959).